Molecular Dynamics Simulation of a Polyunsaturated Lipid Bilayer Susceptible to Lipid Peroxidation

Michal Bachar, Patrick Brunelle, D. Peter Tieleman, and Arvi Rauk*

Departments of Chemistry and Biological Sciences, University of Calgary, Calgary, AB, Canada, T2N 1N4

Received: October 5, 2003; In Final Form: February 9, 2004

Lipid peroxidation is an important part of the pathological pathway of membrane damage in membranes that have high levels of polyunsaturated fatty acids such as linoleic, linolenic, arachidonic, and docosahexaenoic acids. Neural membranes are particularly rich in polyunsaturated acids and such damage is implicated in neurological diseases, such as Alzheimer's disease. To obtain a bilayer model that represents the property of susceptibility to lipid peroxidation, we carried out molecular dynamics (MD) simulations of a bilayer of 1-palmitoyl-2-linoleyl-*sn*-glycero-3-phosphatidylcholine (PLPC). Parameters for the torsional potentials of the *cis*,*cis*-$\Delta^{9,12}$ bis-allylic region of the linoleate chain were fitted to the results of high-level ab initio calculations on model compounds. The MD simulations of the bilayer provided the structural properties of the system and show that the unsaturation induces disorder and affects the physical properties of the membrane.

Introduction

Molecular dynamics (MD) simulations of phospholipid bilayers are widely used to study the physical properties of specific bilayers as well as the bilayer interactions with embedded proteins.[1−11] A biological membrane is a complex mixture of various types of lipids, embedded proteins, and smaller molecules such as oxygen and cholesterol. In recent years, considerable effort has been aimed at developing models that depict more realistically the biological systems, as well as enhancing the accuracy of simulation methods to achieve better agreement with known experimental properties.[12,13] Different lipid compositions have been simulated by a variety of models to study the physical properties of a specific bilayer as well as the bilayer interactions with embedded proteins[4,12−14] and cholesterol.[15]

Interest is growing in the mechanism of lipid peroxidation. Unsaturated lipids are more susceptible to peroxidation than saturated lipids.[16] Studies have been conducted as to the effect of unsaturation on the extent of peroxidation[17] and about the role that peroxidation products play in pathological pathways.[18] Alzheimer's disease (AD) is believed to involve lipid peroxidation as part of its pathology.[19,20] The peroxidation involved in AD is taking place in neuronal cell membranes in the brain. This tissue is sensitive to lipid peroxidation because of high content of polyunsaturated fatty acids (PUFA).[21]

Lipid peroxidation is not likely to occur as a result of reaction with molecular oxygen because of the high activation energy of this process.[22] Rather, lipid peroxidation is believed to be the result of oxidative stress and involves initiation by reactive oxygen and other free radical species. At the atomic level, the most susceptible site for peroxidation is a CH_2 group located between two double bonds.[23] Such a CH_2 carbon is present in the linoleic acid structure at position 11 almost midway down the 18-carbon chain. Thus, to initiate peroxidation, the free radical initiator must reach the hydrophobic core of the lipid bilayer and abstract a hydrogen atom from the carbon atom at position 11, leaving the carbon with an uneven number of electrons.

MD simulations and quantum mechanical (QM) calculations have recently started to address the structures of unsaturated lipids and their bilayers.[24] Huber et al. studied polyunsaturated lipids by applying NMR spectroscopy and MD simulations.[3] Polyallylic docosahexaenoic acid (DHA) chains manifest folded-back structures, which increase the interfacial area per lipid. The values of the order parameter S_{CD} (see below) for the unsaturated chain were significantly lower than one can calculate for fully saturated bilayers. Eldho et al. studied the effect of a loss of a double bond in polyunsaturated bilayers on bilayer physical properties.[1] Feller et al. applied QM calculations to investigate the torsional energy surface for rotation about vinyl−methylene bonds.[2]

Linoleic acid is the simplest fatty acid that contains the multiple double bonds that enhance susceptibility to peroxidation. In this study, we address the details of MD methods to simulate the polyunsaturated lipid system consisting of a bilayer of 1-palmitoyl-2-linoleoyl-*sn*-glycero-3-phosphatidylcholine (PLPC). The principal focus of the present simulations is on the peroxidation site, the *cis*,*cis*-$\Delta^{9,12}$ bis-allylic region of the linoleate chain which includes the target CH_2 group at position 11. The potential energy cost for conformational changes at this site, the resulting geometrical properties of the bis-allylic system, and the distribution in the bilayer will affect its accessibility to oxidizing species and its susceptibility to damage by such species. Hyvönen et al. have already carried out short (1 ns) MD simulations of PLPC using empirical potentials to describe the unsaturated region.[9−11] Their results are relevant to the present study and are discussed below.

As there are no previous reports of Gromacs calculations on systems containing the $-CH_2-CH{=}CH-CH_2-CH{=}CH-CH_2-$ fragment, it was necessary to determine suitable parameters for the Gromos force field to describe the torsional motions. Combining the currently believed mechanism of lipid peroxidation[24] and the atomic details of the system, we attempt to evaluate the MD simulation of PLPC as a model of a bilayer susceptible to peroxidation. Such a model will allow future studies to combine oxidant molecules with the bilayer model and examine the chemistry of such a system using combined quantum mechanical/molecular mechanical (QM/ MM) techniques.

* Address correspondence to this author. E-mail: rauk@ucalgary.ca.

10.1021/jp036981u CCC: $27.50
Published on Web 05/05/2004

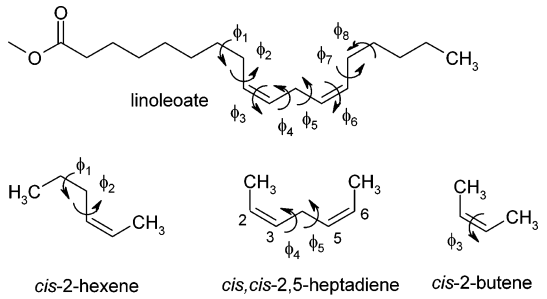

Figure 1. Definition of torsion angles of the unsaturated part of the linoleoate chain for which potential functions were derived. Model systems used for the ab initio potential energy calculations.

Methods

Ab Initio Determination of Parameters. It was necessary to derive and test parameters of potential functions of all eight torsional angles, $V(\phi_1)-V(\phi_8)$, associated with the CH_2-separated cis double bonds. The angles are defined in the linoleate chain in Figure 1.

We assume that $V(\phi_1) = V(\phi_8)$, $V(\phi_2) = V(\phi_7)$, $V(\phi_3) = V(\phi_6)$, and $V(\phi_4) = V(\phi_5)$ because of the approximate symmetry about the central CH_2 (C11) group. Ab initio potential functions were determined at the B3LYP/6-31G(d) level of theory using the Gaussian 98 suite of electronic structure programs.[25] The B3LYP procedure is a hybrid Hartree−Fock/density functional theoretical method specifically designed to achieve experimental accuracy in geometric parameters and relative energies for a wide variety of chemical species.[26] The compounds, *cis*-2-butene, *cis*,*cis*-2,5-heptadiene, and *cis*,*cis*-2,5-nonadiene served as models for the determination of $V(\phi_3)$, $V(\phi_4)$, and $V(\phi_1)$ and $V(\phi_2)$, respectively, as shown in Figure 1. The angles ϕ_1, ϕ_2, and ϕ_4 were scanned in 30° increments over the range −180 to +180°, while ϕ_3 was scanned in 5° increments over the range −50 to +50°. For each angle, all other geometric parameters were optimized. The dihedrals were fitted to a scan of the B3LYP/6-31G(d) vibrationless potential energy surface, optimized every 30 degrees. The fit was performed with OriginPro 7,[27] using the Levenberg−Marquardt method[28] with up to five cosine functions. The Levenberg−Marquardt method is based on the Newton−Gauss method of solving multiple equations with multiple variables from an initial guess. The results from the Levenberg−Marquardt method were adjusted manually to have the minima at 0 kJ mol^{-1}.

Molecular Dynamics Simulation. Molecular dynamics simulations were run using GROMACS 3.1.4.[29] The simulation conditions are similar to the conditions described by Tieleman and co-workers.[30] The neighbor searching was performed using a twin-range approach and 1.0 nm for van der Waals cutoff and electrostatic interactions. Particle mesh Ewald (PME) summation was applied for longer-range electrostatic interactions with a grid spacing of 0.12 nm.[31] The neighbor list update was performed every 10 steps. The time step was 2 fs, using LINCS to constrain all bond lengths.[32] We used NPT conditions (i.e., constant number of particles, pressure, and temperature) in the simulation.[33]

A constant pressure of 1 bar in all three directions was used, with a coupling constant of $\tau_p = 1.0$ ps.[33] This allows the bilayer area to adjust to its optimum value for the force field employed. Water and lipid were coupled separately to a temperature bath at 300 K using coupling constant $\tau_t = 0.1$ ps.

Force Field Parameters. The united atom force field parameters applied were adopted from previous simulations while the torsion parameters unique to the bis-diene moiety were parametrized against ab initio calculations as described above. The lipid parameters related to the headgroups and saturated parts were previously described to produce dipalmitoylphosphatidylcholine (DPPC) properties that are in agreement with experimental results.[34,35] Bond length and bond angle parameters for the two cis double bonds are the same as previously adopted for the single cis double bond of oleic acid[36] in 1-palmitoyl-2-oleoyl-sn-glycero-3-phosphatidylcholine (POPC) bilayers.[37]

The potential due to dihedral angles is taken as a linear combination of terms of the form given in eq 1:

$$V_d(\theta_{ijkl}) = \Sigma_n k_{\theta,n}(1 + \cos(n\theta - \theta_0)) \quad (1)$$

where *i*, *j*, *k*, and *l* are the indeces of contiguous atoms and θ is the angle between the *ijk* and the *jkl* planes. To prevent isomerization of double bonds, a harmonic torsion potential is applied as described in eq 2:

$$V_{id}(\theta_{ijkl}) = k_\theta(\theta_{ijkl} - \theta_0)^2 \quad (2)$$

where $\theta_0 = 0°$ in the case of cis double bonds. The application of all force field elements to MD simulations was previously described in the GROMACS User Manual.[29] The values for all parameters except those derived herein may be found.[34] Explicit formulas used to fit the ab initio potentials are given in the Results section.

Most nonbonded interactions are described as Lennard-Jones interactions. In the present case, because of the comprehensive set of torsion angles used in the fit to ab initio parameters (see below), and the cis nature of the double bonds, the following additional pairs are excluded (decadiene numbering): (2,7), (2,8), (3,7), and (3,8). For the linoleic chain, the equivalent pairs were excluded.

***cis*,*cis*-3,6-Decadiene−Single Molecule Simulation.** A single *cis*,*cis*-3,6-decadiene molecule was first minimized applying a steepest descent algorithm and then equilibrated in vacuo by a stochastic dynamics (SD) simulation. SD calculations allow one to simulate a macromolecule in vacuo. The atomic friction coefficient γ_i has a specific value for each atom.[6] The lipid force field[34] including its Lennard-Jones parameters were applied to the isolated decadiene molecule.

***cis*,*cis*-3,6-Decadiene−Equilibrated Box Simulation (Liquid Phase).** The initial structure was an equilibrated box of 512 decane molecules. The saturated sections at C3−C4 and C6−C7 were converted to double bonds. First, the box was minimized applying a steepest descent algorithm, and then equilibrated by molecular dynamics using an earlier version of the force field. Neighbor searching was performed using a twin-range cutoff with neighbor list cutoff 1.0 nm and Coulomb cutoff 1.0 nm with a grid spacing of 0.12 nm.[31] As in the single molecule case, the lipid force field[34] including its Lennard-Jones parameters were applied to the simulation of liquid decadiene. The decadiene box was equilibrated for a further 20 ns and the production run lasted 80 ns more. NPT conditions, with a constant pressure of 1 bar in all three directions, were used, with isotropic type coupling and a coupling constant of $\tau_p = 1.0$ ps.[33] This allows the decadiene box area to adjust to its optimum value for the force field employed. The decadiene molecules were coupled to a temperature bath at 300 K using coupling constant $\tau_t = 0.1$ ps.

Bilayer Simulation. NPT conditions were applied. A constant pressure of 1 bar in all three directions was used, with anisotropic coupling and a coupling constant of $\tau_p = 1.0$ ps.[33] The anisotropic coupling allows the system to adjust its area in

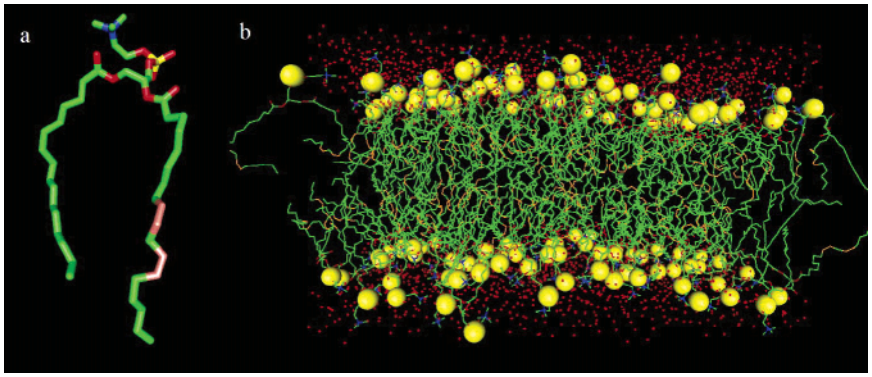

Figure 2. **(a)** Individual lipid from the equilibrated system. The atoms in the unsaturated area are labeled. Colors: cyan, SP2 atoms C9, C10, C12, and C13; green, SP3 carbons; yellow, the SP3 carbon between the double bonds, C11. **(b)** A snapshot of the system during the production run. The phospholipids are presented as a whole molecule in the cases where they are out of the simulation box. Atom labeling as in **(a)**.

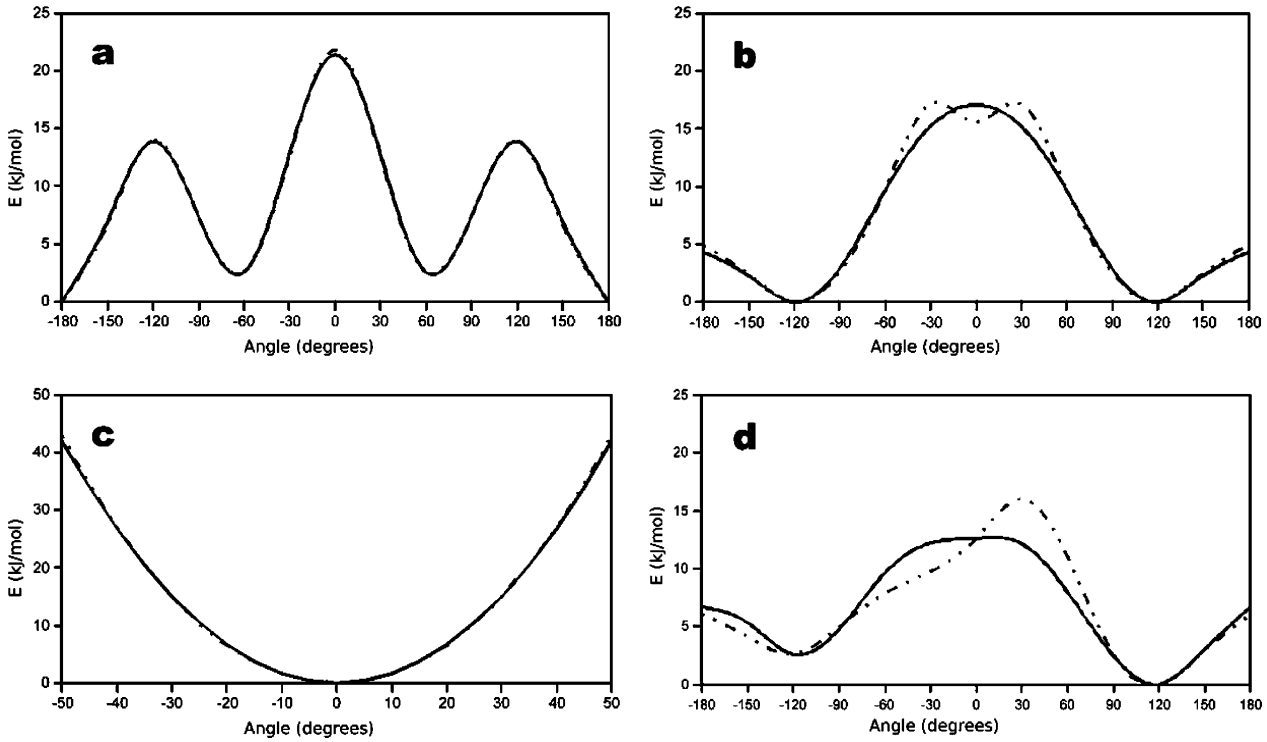

Figure 3. Fit of the parametrization (solid line) to the ab initio potential (dashed line). Refer to Figure 1 for definitions: (a) $V(\phi_1)$ (=$V(\phi_8)$); (b) $V(\phi_2)$ (=$V(\phi_7)$); (c) $V(\phi_3)$ (=$V(\phi_6)$); (d) $V(\phi_4)$ (=$V(\phi_5)$).

the *xy* plane independently of the *z* direction (the direction of the bilayer normal). This allows the bilayer/peptide area to adjust to its optimum value for the force field employed. Water and lipid were coupled separately to a temperature bath at 300 K using coupling constant $\tau_t = 0.1$ ps. The water model used was SPC.[29,38]

Initial structure. The PLPC bilayer initial structure was adapted from POPC bilayer coordinates.[39] It was partially minimized using a steepest descent method for 1000 steps, and then fully equilibrated to adjust bond lengths, angles, and dihedrals to convert the saturated C11−C14 segment into the additional double bond in each phospholipid. The bilayer contained 128 molecules of PLPC and 2453 water molecules (water/lipid ratio = 19.2). The equilibration of the system lasted 10 ns and the production run lasted 50 additional ns. Figure 2a shows the structure of a randomly chosen individual lipid in the equilibrated system and Figure 2b shows a snapshot of the equilibrated PLPC bilayer.

Results

Parametrization. The ab initio potentials of the model systems are plotted as dashed lines in Figure 3.

These were fitted with the following potential functions:

$$V(\phi_1) = 3.350[1 + \cos(\phi_1)] - 1.660\,[1 + \cos(2\phi_1 - 180)] + 7.333\,[1 + \cos(3\phi_1)] \quad (3)$$

$$V(\phi_2) = -5.685 + 7.470\,[1 + \cos(\phi_2 - 180)] + 3.900\,[1 + \cos(2\phi_2)] + 1.100\,[1 + \cos(3\phi_2 - 180)] \quad (4)$$

$$V(\phi_3) = 0.034617\,[\phi_3]^2 \quad (5)$$

$$V(\phi_4) = -5.300 + 4.533\,[1 + \cos(\phi_4 - 180)] + 3.000\,[1 + \cos(2\phi_4)] + 1.550\,[1 + \cos(3\phi_4 - 180)] + 1.300\,[1 + \cos(\Theta)] \quad (6)$$

where ϕ_1−ϕ_4 are defined in Figure 1 and Θ is the torsion angle between the vectors defined by the two double bonds (C4−C3

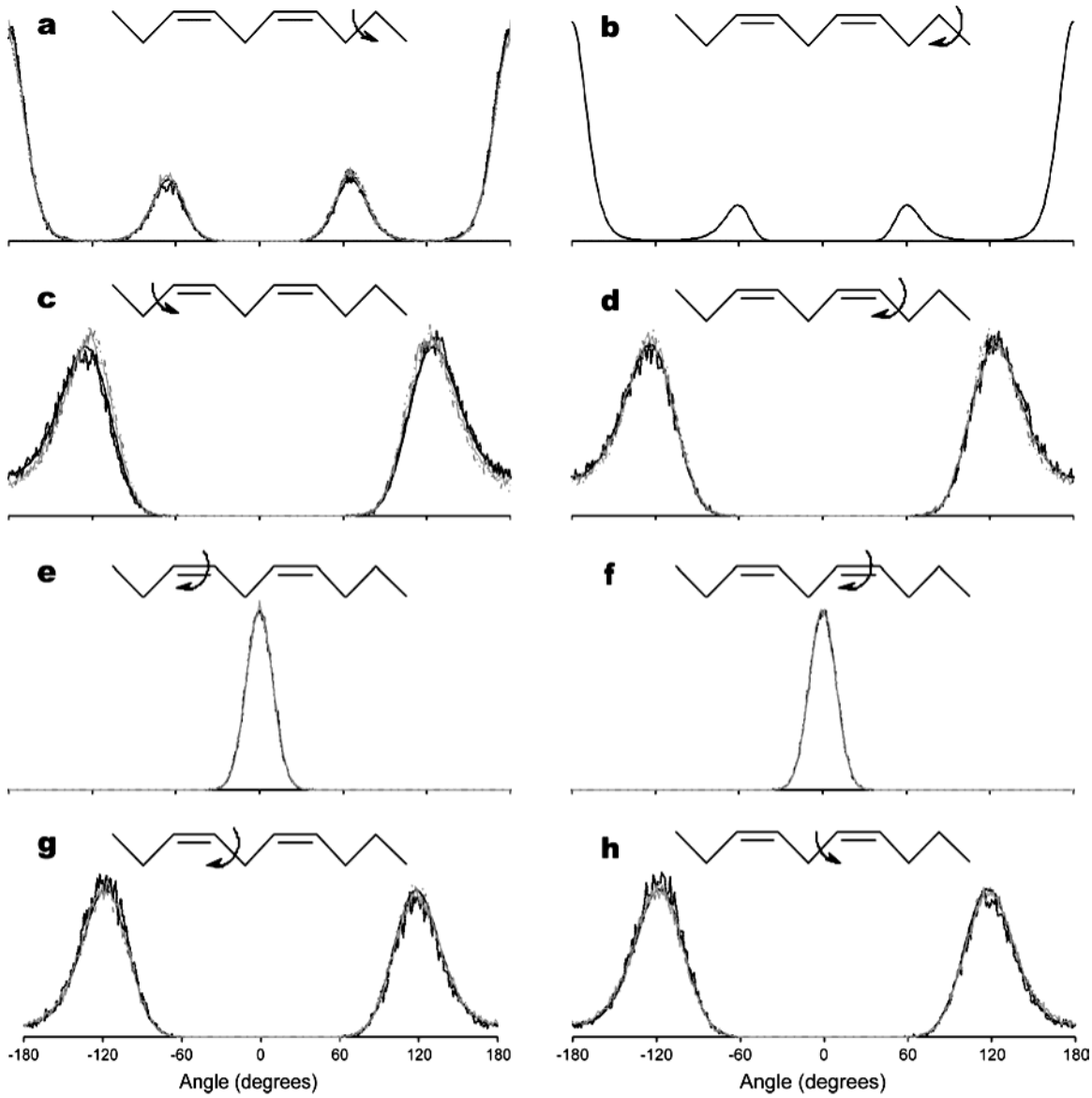

Figure 4. Normalized distribution for *cis,cis*-3,6-decadiene in vacuo (dashed gray line), one randomly chosen *cis,cis*-3,6-decadiene molecule (#312) in liquid (solid gray line), one randomly chosen lipid molecule (#27) in the PLPC bilayer (dashed black line), and the average of all lipid molecules (solid black line): (a) V(ϕ_8); (b) V(ϕ_8); (c) V(ϕ_2); (d) V(ϕ_7); (e) V(ϕ_3); (f) V(ϕ_6); (g) V(ϕ_4); (h) V(ϕ_5).

and C6−C7, in the *cis,cis*-3,6-decadiene; C10−C9 and C12−C13, in the linoleoate chain). All angles are in degrees and the potential V is in kJ mol^{-1}. These potentials were used for the *cis,cis*-3,6-decadiene systems as well as for the bilayer.

The fitted Gromacs potentials (eqs 4−7) are plotted as solid lines in Figure 3. The fit is excellent in V(ϕ_1) (Figure 3a) and V(ϕ_3) (Figure 3c). The standard deviations from the ab initio potentials are 0.14 kJ mol^{-1} and 0.32 kJ mol^{-1}, respectively. To reduce the complexity of the potential functions in V(ϕ_2) (Figure 3b) and V(ϕ_4) (Figure 3d), emphasis was placed on fitting the shape of the potential near the minima and the lower barrier at $\phi = 180°$. It was evident from the ab initio calculations that V(ϕ_4) had a secondary dependence on the value of ϕ_5. The curve shown in Figure 3d corresponds to $\phi_5 \approx 120°$. The lower minimum at $\phi_4 = 120°$ corresponds to a structure of *cis,cis*-2,5-heptadiene with C_2 symmetry, while the structure at $\phi_4 = -120°$ has C_s symmetry and is 2.6 kJ mol^{-1} higher. With $\phi_5 \approx -120°$, the positions of the minima in Figure 3d are reversed and correspond to C_2-like and C_s-like geometries with (ϕ_4, ϕ_5) = (−120°, −120°) and (120°, −120°), respectively. The dependence of V(ϕ_4) on the value of ϕ_5 is accomplished by defining a dependence on the angle of twist between the vectors defined by the two double bonds as specified in eq 6. The analogous definition for V(ϕ_5) incorporates the secondary dependence on ϕ_4 in a parallel manner. The standard deviations from the ab initio potentials for V(ϕ_2) and V(ϕ_4) are 0.22 kJ mol^{-1} and 0.98 kJ mol^{-1}, respectively, excluding the higher energy region between −60° and +60°.

Distribution Functions of the Unsaturated Moiety. The potentials given by eqs 3−6 and shown in Figure 3 give rise to the angular distribution curves shown in Figure 4. Except in Figure 4b, each of the plots in Figure 4 is a superposition of four curves, an isolated decadiene in vacuo, a randomly chosen decadiene molecule in the liquid phase simulation, a randomly chosen PLPC molecule in the bilayer simulation, and the average of all corresponding bonds in the PLPC bilayer simulation. For comparison with the distribution on angle ϕ_8 (or ϕ_1), the analogous distribution for rotation about the C15−C16 bond (of type CH2−CH2−CH2−CH2) is shown in Figure 4b.

Structural Properties. In biological systems, the density, thickness, and the area per headgroup is a function of different lipid composition as well as embedded proteins.[1,40]

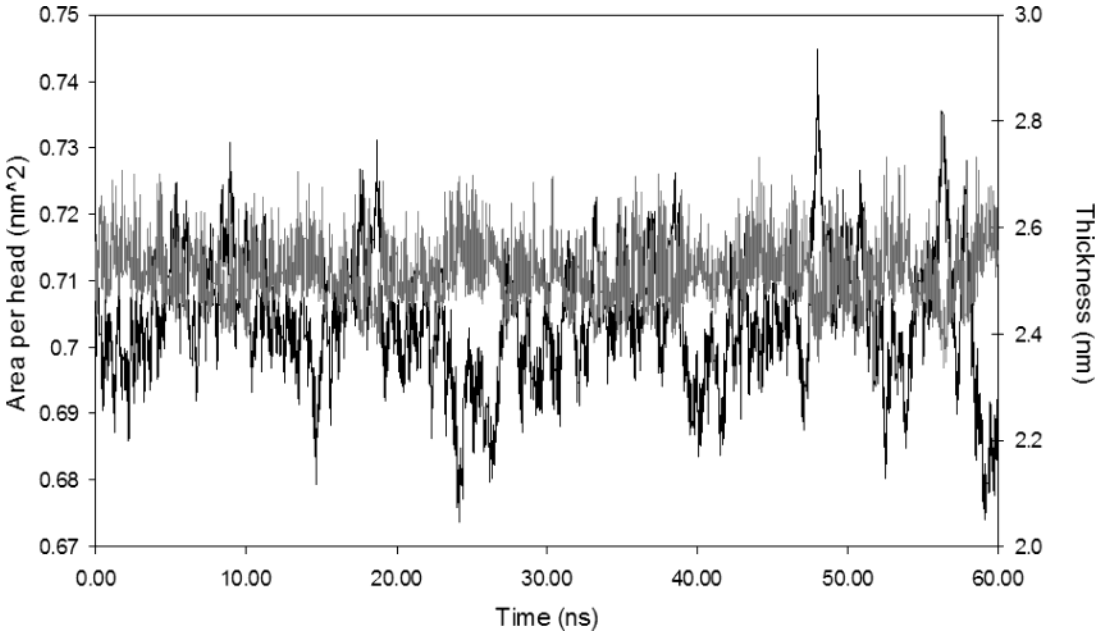

Figure 5. Area per headgroup (left scale and black lines) and hydrophobic thickness (right scale and gray lines) during the entire 60 ns of the simulation.

The thickness of the PLPC membrane, measured as the average distance between opposite acyl carbon atoms (C1), is plotted as a function of simulation time in Figure 5. As shown in Figure 5, the average fluctuates over a narrow range. The time-averaged thickness was 2.506 ± 0.054 nm. The average area per headgroup was ⟨0.703⟩ ± 0.010 nm^2, calculated for snapshots taken every 5 ps during the 50 ns of the production run. As shown in Figure 5, the area per headgroup fluctuates over the range of 0.68−0.73 nm^2.

The bilayer density profile and distribution of selected groups presented in Figure 6 was averaged for the last 50 ns of the production run and calculated every 1 ps. Results are plotted relative to the center of the bilayer along the bilayer normal (*z*-axis). The peak-to-peak separation of the charged phosphate groups is 3.5 nm (Figure 6 top curves). The water distribution penetrates past the phosphate groups and drops to zero shortly thereafter, leaving a region 2.4-nm thick in the interior from which water is excluded (Figure 6 top curves). The unsaturated moiety, CH2−CH═CH−CH2−CH═CH−CH2, is represented by the "CH" group in Figure 6 (top). To gain a better insight into the location of the individual double bonds and the central CH_2 group, these are individually plotted in Figure 6 (bottom curves). Each has a nearly symmetrical Gaussian-like distribution. The CH_2 group (C11) remains almost entirely in the water-free region of the membrane and its distribution overlaps considerably with the distribution of the terminal CH_3 groups (compare top and bottom curves of Figure 6).

Deuterium Order Parameter, S_{CD}. MD simulations of lipid bilayers permit one to assess the extent of order against experiment in the form of the deuterium order parameter, S_{CD}, which is related to the measured quadrupolar splitting, $\Delta\nu_Q$, in an axially averaged line shape:

$$\Delta\nu_Q = 3/4\,(e^2qQ/h)S_{CD} \tag{7}$$

where the term in parentheses is the quadrupolar coupling constant. From the MD simulation, S_{CD} is derived from

$$S_{CD} = \langle 3/2\cos 2\theta - 1/2\rangle \tag{8}$$

where θ is the angle between the bilayer normal and the C−H bond vector and the brackets denote an average over all lipids and over the time of the simulation.

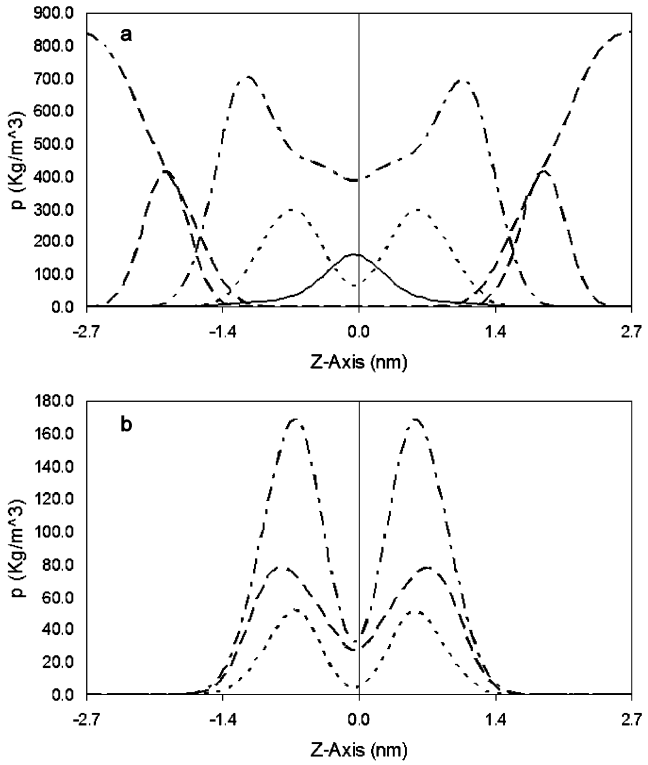

Figure 6. Mass density profiles: (a) CH_3 groups (____), PO4 groups (peak at ±1.7, - - - -), water (starts high at edges, - - - -), CH_2 groups (- · - · - ·), "CH" groups (· · · · ·); (b) CH_2 group (C11,· · · · ·), CH_2 groups (C8 and C14, - - - -), CH groups (C9, C10, C12, and C13, - · - · - ·).

Measurements of S_{CD} were conducted for POPC bilayers and polyunsaturated lipid bilayers.[3] Such spectroscopic measurements indicate that cis double bonds enhance the disorder to a greater extent than trans double bonds, and a lower order within the hydrophobic core is observed. The deuterium order parameter, S_{CD}, is also an indicator of the fluidity of the bilayer. Figure 7 describes the S_{CD} values for the saturated and unsaturated

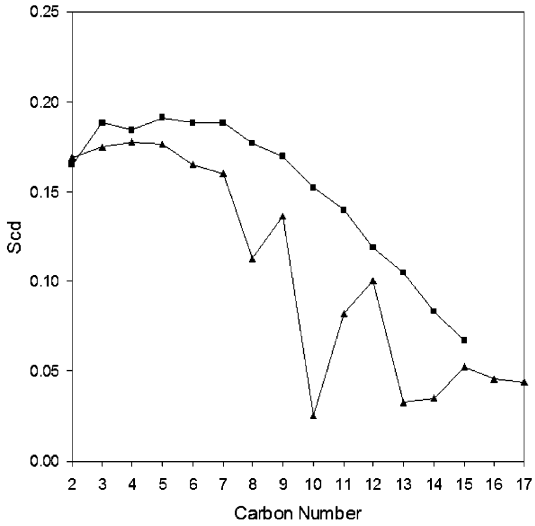

Figure 7. Deuterium order parameter. The S_{CD} was calculated over the 50 ns of production run and averaged every 1 ps.

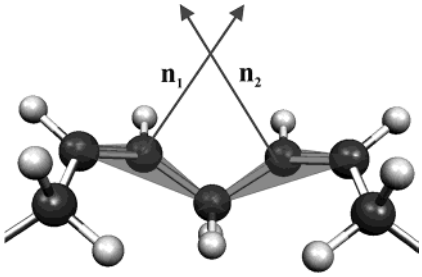

Figure 8. Angle θ, is the angle between the normals of the planes formed by two groups of three atoms: C9, C10, C11 and C13, C12, C11: $\theta = \text{acos}(\mathbf{n}_1.\mathbf{n}_2)$. The unsaturated part of the linoleate chain is modeled here by *cis*,*cis*-2,5-heptadiene for clarity.

chains separately. The highest order for the saturated chain, $S_{CD} = 0.18-0.19$, occurs from C3−C9 and decreases monotonically down the chain to its lowest value, $S_{CD} = 0.07$. Considerably more fluctuation is observed in the unsaturated chain. The maximum, $S_{CD} = 0.18$, is similar to the saturated chain but the order parameter drops rapidly to lows at the unsaturated linkages, C10 ($S_{CD} = 0.02$) and C13 ($S_{CD} = 0.03$) with a small rises at C11 ($S_{CD} = 0.08$) and C12 ($S_{CD} = 0.10$). From C14−C17, consistently low values, $S_{CD} \approx 0.04$, are achieved.

Tilt of the Lipids. The tilt was calculated as the angle that the averaged C1-to-C*n* vector makes with the membrane normal. Calculating the lipid tilt for the last 50 ns of the production run resulted in a value of 34.8° ± 18.3° for the *sn*-2 chain and 1.6° ± 4.2° for the *sn*-1 chain.

Planarity of the Peroxidation Site. Abstraction of an H atom from C11 to initiate lipid peroxidation is most readily accomplished if the parent 1,4-diene moiety is already quasiplanar. To evaluate the planarity in the system, we defined the angle θ as the angle between the normals of the planes formed by two groups of three atoms: C11, C10, C9 and C13, C12, C11 (Figure 8). The angle for a randomly chosen lipid in the PLPC bilayer simulation was calculated every 1 ps over the last 50 ns of the production run and the distribution of values is depicted as the bold solid line in Figure 9.

A value of $\theta = 0°$ corresponds to a "w" conformation of the bis-allylic system. For values near $\theta = 0°$, the chain is maximally extended. The value $\theta = 0°$ itself is improbable because of steric interactions between the H atoms at C10 and C12 (according to the ab initio calculations). At the other extreme, a value of $\theta = 180°$ corresponds to a sicklelike

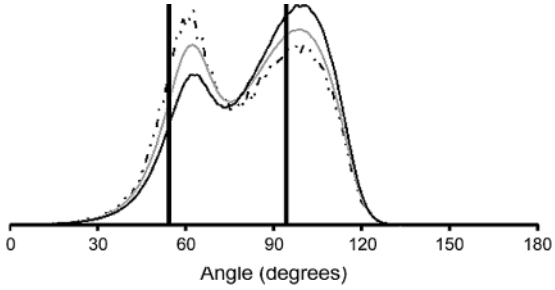

Figure 9. The normalized distribution of the angle, θ, between planes (see Figure 8): single lipid in the bilayer (_____); single. The values of θ for two conformations of 2,5-heptadiene are shown by the bold vertical lines, C_s (left) and C_2 (right).

conformation in which the chain is folded back on itself. The actual value, $\theta = 180°$, is strongly forbidden because it involves a very close approach of the C10 and C14, or C8 and C12, atoms.

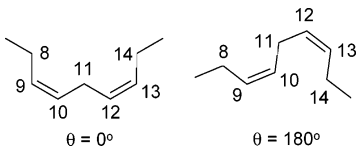

The distribution in Figure 9 shows two peaks close to the two minimum energy conformers found by the ab initio calculations on *cis*,*cis*-2,5-heptadiene, shown by the bold vertical lines. The conformer of *cis*,*cis*-2,5-heptadiene with C_2 symmetry ($\theta = 94°$) is lower than the conformer with C_s symmetry ($\theta = 54°$) by 2.6 kJ mol^{-1}. The vacuum distribution of a single *cis*,*cis*-3,6-decadiene molecule, shown as the dotted line in Figure 9, has a lower broader peak at 100° (C_2-like) and a higher sharper peak at 60° (C_s-like). The solid gray line in Figure 9 is the corresponding plot for a single *cis*,*cis*-3,6-decadiene molecule in the liquid-phase simulation. The peak maxima in the distribution are unaffected by the change of state from vacuum to liquid but the population shifts toward the C_2-like structures. The ratios of the total populations of C_2- and C_s-like structures are $[C_2]/[C_s] = 0.64/0.36$ (vacuum) and $[C_2]/[C_s] = 0.70/0.30$ (liquid). It is evident from Figure 9 that the effect of the bilayer structure is to shift the population further toward the C_2-like structures, $[C_2]/[C_s] = 0.76/0.24$ (bilayer).

Discussion

The purpose of simulating a single molecule (of *cis*,*cis*-3,6-decadiene) was to apply the new parameters to a less-complex system which has all of the features of the bis-diene moiety of linoleic acid but does not include intermolecular interactions. The single molecule simulation established reference torsional distribution functions for all of the angles associated with the two-double-bond grouping free of any medium effects. Comparison with distribution functions derived from the liquid-phase simulation permits detection of any effects due to the condensed state, and comparison with single lipid (in the bilayer) and average bilayer distribution functions permits elucidation of effects specific to the anisotropic environment of the bilayer. All of the distribution functions for all of the important angles are shown in Figure 4. The four cases for rotation about the torsion angle ϕ_8 (or ϕ_1) in Figure 4a are essentially superimposable, indicating that the environment of the molecule, whether vacuum, liquid, or bilayer, has virtually no effect on the distribution about this saturated bond. In each case, the anti/gauche ratio is 65.5/34.5. Figure 4b shows the analogous

distribution about a bond which is typical of the palmitoyl chain and the fully saturated segments of the linoleyl chain. The difference in populations of anti and gauche conformers is apparent from inspection. Integration yields the ratio anti/gauche = 78.4/21.6.

Figure 4c and 4d compares the population distributions about the outside single bonds that terminate in sp^2 hybridized carbon atoms. The curves peak near the minima of the potential curves $V(\phi_2)$ in Figure 3b but there is a significant population of the planar form at $\phi_2 \approx 180°$ that corresponds to the low barrier.

Figure 4e and 4f shows the distribution of the twist angle at the two double bonds. There is no discernible difference between the two double bonds in any of the four cases; the isolated *cis*,-*cis*-3,6-decadiene distribution is the same as that of one lipid or the average of all in the PLPC bilayer.

Figure 4g and 4h shows the distribution about each of the single bonds to the central CH_2 group (C11), ϕ_4 and ϕ_5. Again, the curves for the four cases are almost superimposable, indicating no medium effects on the distribution of conformers. As in the rotation about ϕ_2 (Figure 4c) and ϕ_7 (Figure 4d), the distribution is peaked about the minima in the potential energy curve (Figure 3d).

Bilayer Properties. Increasing chain length causes membrane thickening, whereas increased chain unsaturation or strength of headgroup repulsions causes the bilayer to thin when the headgroup is the same. The grid-based simulation study of Cantor[40] includes a description of pressure as a function of double-bond location in the chain. Apparently, the closer the double bond is to the headgroup, the stronger the pressure applied. A double bond located in position 9 is less effective in applying a significant change in pressure, yet the occurrence of two double bonds (positions 9 and 12) is expected to have a cumulative effect. Such an effect is expected to increase the area per headgroup in a 9,12-unsaturated lipid bilayer as opposed to the area per headgroup calculated for a saturated bilayer such as DPPC.

Density Profile. Membranes with an unsaturated chain are expected to equilibrate into more disordered systems than fully saturated membranes because of the kinks introduced by the cis double bonds. This results in a broader peak in the distribution function for different groups, a larger area per headgroup, and lower values of the order parameter, S_{CD}. These effects are magnified in the present system, which has two cis double bonds per lipid. For instance, while the profile presented in Figure 4 is in general agreement with previous studies for the distribution of headgroups, water, and terminal CH_3 groups,[41] a wider distribution of the terminal CH_3 groups is obtained for our PLPC bilayer than was observed for DOPC bilayers.[41]

Area per Headgroup and Hydrophobic Thickness. Since unsaturated bilayers have recently been applied to study membrane-embedded proteins, the area per headgroup has been presented in many previous studies.[5,42−44] The average area per headgroup calculated for PLPC is consistent with the values calculated in the previous studies. The value $\langle 0.70 \rangle$ nm^2 is larger than calculated for the L_α phase of DPPC bilayers, 62−68 nm^2,[5] yet smaller than calculated for 18:2 bilayers (containing only unsaturated lipids), 70−72 nm^2.[5] Simulating the bilayer with anisotropic pressure conditions allows the system to expand or shrink independently in the *z* direction (thickness) and in the *xy* plane (area per headgroup).

The hydrophobic thickness, $2D_C$,[45] calculated as the separation of the acyl carbons of the hydrophobic chains, was 2.5 nm. Previous experimental studies of a DHA bilayer indicate a hydrophobic thickness of 3.05 nm.[1] For a saturated bilayer (DPPC), the value for the hydrophobic thickness is lower (about 3.0 nm).[45]

The distance between the maxima in the mass density profile for the PO4 group was 3.5 nm. Hyvönen et al. began their simulation of PLPC with a similar value but achieved an average value of 4.16 nm during their 1 ns simulation.[9] According to Saiz and Klein,[7] the electron density profile for the PO4 group shows a separation of 4.33 nm for a bilayer of 18:0/22:6. On the other hand, Huber et al. report a headgroup distance of 3.5 nm for a 1-palmitoyl-2-docosahexaenoyl-sn-glycero-3-phosphocholine (16:0/22:6) bilayer.[3] Our results indicate that the presence of an unsaturated region with low barrier torsion angles allows conformations in which the chain is folded back, as previously found,[2] resulting in a relatively low thickness. This flexibility accounts for the fluctuations in the thickness as well as for the variability in area per headgroup.

Density and Fluidity. The density profile shown in Figure 6 has features in common with previous studies.[41] The "CH" group marks the area where the system density is lower and remains low down to the CH_3 groups. Both the presence of the double bonds and the mismatch between the *sn*-1 and *sn*-2 chains contribute to the lower density in the vicinity of the CH_3 groups. Although the double bonds tend to decrease flexibility, the low barrier torsion angles, in the surrounding region, increase flexibility and conformational changes. The low values obtained in the S_{CD} calculation, indicate that some of the unsaturated chains are folding backward.[2] By adopting such conformations, the fluidity is expected to increase and density to decrease. Such conformations might account for the wide distribution of the unsaturated region, overlapping the CH_3 group region.

An oxidizing free radical passing through such a system may migrate faster in this zone or have a higher solubility than in the saturated areas closer to the heads. The more fluid environment may also affect its conformation. Thus, in addition to the chemical properties of the allylic system, the local disorder of the unsaturated zone may enhance the reactivity toward effecting peroxidation.

The Deuterium Order Parameter, S_{CD}. To begin the peroxidation process, the initiator molecule has to migrate into the hydrophobic core to reach the C11 carbon. Thus, order properties of the system should have a bearing on the degree of susceptibility to peroxidation. The area per headgroup is very strongly related to the order parameter calculated for a bilayer.[3] Previous MD studies report lower S_{CD} values for the *saturated* chain of POPC than observed for fully saturated lipids (DPPC).[46] The greater disorder for the saturated chain of POPC was attributed to the presence of the unsaturated chain. Contrary to earlier work,[47] the more recent NMR study of Holte et al. confirms this effect.[48] The experimental S_{CD} distributions for the saturated chains of POPC were similar to the numbers obtained in the present study and shown in Figure 7.

Experimental studies[47] and previous simulations of DOPC[41,49] exhibited a characteristic dip at carbon 10 of the oleic acid chains. Our PLPC bilayer also shows the same features. The S_{CD} value starts to drop at C7, rises at C9, and has a deep minimum at C10. As for the saturated chain, the values are lower than shown for DPPC simulations in the terminal region. Apparently, unsaturation in *sn*-2 causes a decrease in *sn*-1 chain order that is largest toward the end of the chain. The increase in disorder accounts for the increased value in area per headgroup. The values obtained are in agreement with previous simulations. Huber et al. show a similar drop in S_{CD} value in C9 of POPC.[3] The polyunsaturated chains, studied by Huber et

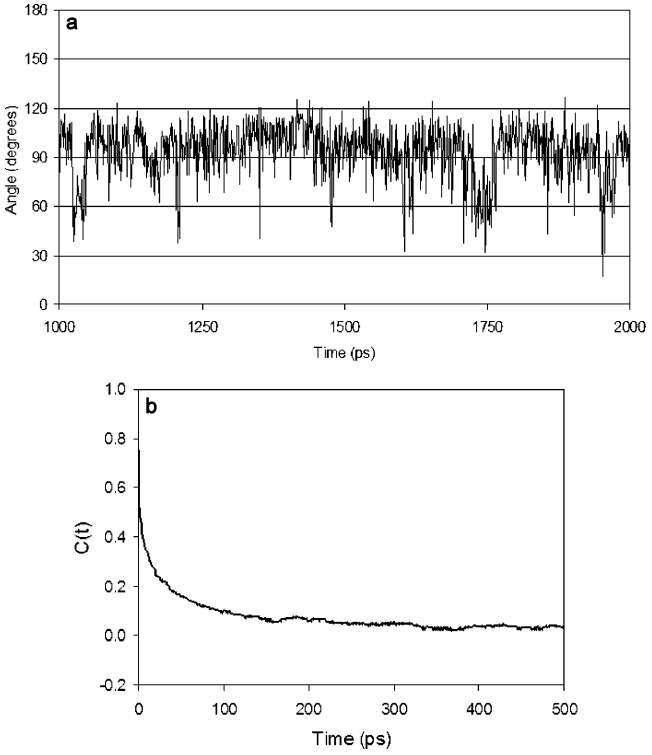

Figure 10. (a) Value of θ for a single lipid in the bilayer followed for 1 ns. (b) Correlation function for θ.

al., show even a larger extent of disorder than seen for PLPC.[3] Evidently, the more unsaturated bonds reside in the chain, the more disordered it becomes.

The present results can be compared directly with the previous 1-ns simulation of PLPC by Hyvönen and co-workers.[9] The S_{CD} values achieved in their short simulation differ markedly in several respects from Figure 7: their saturated chain had a similar value to ours at C2 but peaked at a higher value at C6, $S_{CD} = 0.22$; their unsaturated chain started at a very low value ($S_{CD} = -0.05$) at C2, had a minimum at C11 instead of C10, and did not rise at C12. We attribute these differences to a lack of equilibration in the short time frame.

Tilt of the Lipids. The averaged orientation of the saturated *sn*-1 chain of PLPC in the bilayer was nearly coincident with the bilayer normal. The average tilt is $1.6° \pm 4.2°$. This result is in sharp contrast to that found for the unsaturated *sn*-2 chain, for which a tilt of $34.8° \pm 18.3°$ is calculated. The latter result is similar to that found by Hyvönen and co-workers, 38°.[9] However, the *sn*-1 chain tilt differs markedly from theirs, 27°, possibly because of the 1-ns simulation time.

Structural Properties and the Potential for Peroxidation. The overall effect of the linoleic chain is a less dense and less ordered system than is the case for bilayers with single double bonds or none. This disorder may increase access to the peroxidation site of reagents that could initiate lipid peroxidation.

The mechanism of lipid peroxidation is described in Figure 11. The crucial first step in the lipid peroxidation process is the formation of a pentadienyl radical. This radical then rapidly reacts with molecular oxygen dissolved in the hydrophobic part of the bilayer in a sequence of steps that results in chain cleavage and formation of toxic substances such as 4-hydroxynonenal and other unsaturated aldehydes.[20]

The local geometry of the *cis*,*cis*-bis-allylic system is of particular interest since such systems are reported to have relatively low bond dissociation energies for abstraction of hydrogen atoms from the central CH_2 group (C11).[24] This low

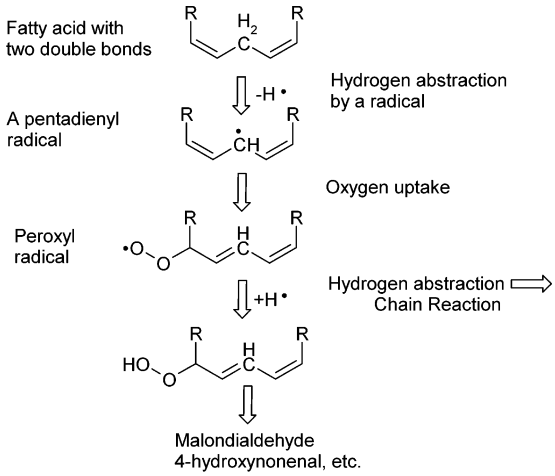

Figure 11. The initial steps in the mechanism of lipid peroxidation.

bond dissociation is due to the ability of the adjacent double bonds to stabilize the radical by delocalization. The stabilization is greatest when the double bonds and the carbon between them form a planar system. The most stable form of the initially formed conjugated radical (a pentadienyl radical analog) is the planar "w" conformation and corresponds to $\theta = 0°$ as defined in Figure 8.[50] In the 1,4-diene system that gives rise to the pentadienyl radical, four conformations in the region of the double bonds may be distinguished. In the notation of Hyvönen and co-workers,[9] there are two "C_2"-like conformers, PP (ϕ_4 and ϕ_5 both positive) and MM (ϕ_4 and ϕ_5 both negative), and two "C_s"-like conformers labeled by analogy as PM and MP. The two "C_s"-like conformers are less stable than the two "C_2"-like conformers by 2.6 kJ mol^{-1} according to V(ϕ_4) and V(ϕ_5). However, because of the presence of the chiral center in the glycerol moiety, the PP and MM pair are diastereomeric and would be expected to have different populations in principle, as would the PM and MP pair. In the lipid bilayer, two issues arise: first, to what extent does the single remote chiral center induce asymmetry and therefore unequal populations in the (PP, MM) and (PM, MP) pairs; second, is there a significant effect of the bilayer on the distribution of more planar forms of the four structures? If so, this would indicate a greater propensity toward peroxidation. We address these questions separately below.

In their 1-ns simulation of PLPC, Hyvönen, and co-workers[9] found substantial differences in the total populations of the four conformers of the unsaturated region: PP, 32%; MM, 39%; PM, 9%; MP, 19%. In our 50-ns simulation, we find similar inequalities in the case of a single randomly chosen lipid (PP, $38\% \pm 5\%$; MM, $45\% \pm 8\%$; PM, $8\% \pm 5\%$; MP, $9\% \pm 3\%$) but far smaller differences when averaged over all lipids (PP, $38.2\% \pm 0.7\%$; MM, $38.2\% \pm 0.6\%$; PM, $11.7\% \pm 1.0\%$; MP, $11.9\% \pm 0.7\%$). The error bars correspond to the range of values observed in the averages within individual 10-ns segments of the total 50-ns simulation time. Two conclusions follow from these results: (1) population differences in the (PP, MM) pair and the (PM, MP) pair are not statistically significant—the influence of the asymmetry of the glycerol moiety is not felt as far away as the double-bond region; and (2) while the average conformations (and presumably other properties) of the bilayer are well equilibrated after the initial 10 ns, this is not true of individual lipids even after 60 ns.

On the question of planarity and susceptibility to peroxidation: the angle, θ, between the planes of the two double bonds (Figure 8) serves as a measure of the planarity of the five-carbon

unsaturated region. A value of $\theta = 0°$ would correspond to the geometry of the most stable pentadienyl radical that could be reached by abstraction of one of the H atoms from C11. As seen in the distribution of θ values in Figure 9, there is a rather low probability for structures with $\theta < 40°$, which corresponds approximately to a *simultaneous* deviation of about 30° from planarity in the torsion angles, ϕ_4 and ϕ_5, in the more abundant "C_2"-like conformers, PP and MM. Inspection of Figure 4g and 4h shows that there is a non-negligible population of structures where one of the double bonds is coplanar with the first C atom of the other ($\phi_4 = 180°$, $\phi_5 \approx \pm 120°$, or $\phi_5 = 180°$, $\phi_4 \approx \pm 120°$). Such "half-planar" structures are not reflected in Figure 9 since in each case $\theta \approx 60°$. The time-dependent behavior of θ in a single lipid, shown in Figure 10 (top graph), reveals numerous short-lived excursions to low θ values even on a 1-ns time scale. The autocorrelation function of θ, shown in Figure 10 (bottom graph), drops to zero after only 200 ps. This is indicative of a fast process that scrambles the planarity measure but does not imply that conformational equilibrium is established on this time scale.

Conclusions

Molecular dynamics simulations using Gromacs were applied to obtain a bilayer consisting of 1-palmitoyl-2-linoleoyl-*sn*-glycero-3-phosphatidylcholine (PLPC). The PLPC bilayer is the simplest bilayer that has the 1,4-unsaturation necessary for efficient lipid peroxidation. Ab initio calculations at the B3LYP/6-31G(d) level were used to obtain accurate potential functions for the 1,4-unsaturated region. Independent MD simulations on a model system, *cis,cis*-3,6-decadiene both in vacuo and as a liquid, and on the PLPC bilayer, revealed that there are almost no effects of the medium on the distribution of rotamers about any of the bonds. However, the population of C_2-like structures in the double-bond region increased at the expense of C_s-like structures in liquid decadiene compared to the isolated molecule case, and this trend was magnified in the PLPC bilayer. The relative populations of the pair of C_2-like structures and the pair of C_s-like structures were monitored to detect the presence of long-range asymmetry induced by the chiral center in the glycerol moiety. The populations of the two pairs were the same to within statistical significance. Thus, the time-averaged environment in the region of the double bonds is not unsymmetrical.

The MD simulation of the PLPC bilayer lasted 60 ns. Data were collected during the last 50 ns on a single randomly selected lipid as well as averaged over the entire 128 lipids of the bilayer. Using the populations of the C_2- and C_s-like structures as a measure, it was evident that the average properties of the bilayer were well equilibrated after 10 ns but that individual lipid properties were not, even after 60 ns. The following observations pertain to properties averaged over the whole bilayer.

The structural characteristics of the PLPC bilayer are in the range of those observed experimentally or in MD simulations on other bilayers. The hydrophobic thickness (distance between opposite acyl C atoms) is 2.506 nm. The average separation of PO4 groups is 3.5 nm. The average area per headgroup is 0.70 nm^2. The density distribution of the unsaturated region in the hydrophobic core is low (about 700 kg m^{-3}). The deuterium order parameter (S_{CD}) of the saturated *sn*-1 chain is somewhat lower than observed for less saturated bilayers and S_{CD} of the unsaturated *sn*-2 chain has the characteristic minimum at C10 of the first double bond and low values for the part of the chain beyond the second double bond. Very different average tilt angles were found for the *sn*-1 and *sn*-2 chains, 1.6° ± 4.2° and 34.8° ± 18.3°, respectively.

The unsaturation of PLPC enhances its susceptibility to lipid peroxidation because it incorporates the 1,4-diene moiety from which a stable pentadienyl radical can be generated by oxidation. The structural properties of the PLPC bilayer were analyzed for details of the physical environment that an oxidizing agent might experience in the hydrophobic region as well as the geometrical properties of the site where peroxidation would be initiated. The anisotropic environment of the bilayer interior does not induce any global shift to more planar structures that would be more susceptible to radical generation. However, the dynamics indicate that frequent excursions to more planar structures occur even on a 1-ns time scale. Compared to less unsaturated bilayers, the PLPC bilayer is more disordered, particularly in the hydrophobic region between the headgroups and the bis-allylic methylene groups. This disorder (or fluidity) may enhance the opportunity of an external agent to diffuse into that region.

Acknowledgment. The financial assistance of the Natural Sciences and Engineering Research Council of Canada and of the Alzheimer's Society of Canada is gratefully acknowledged. One of us (M.B.) is grateful for a Fellowship from the Alberta Ingenuity Fund. P.B. is grateful for a Scholarship from the Alberta Ingenuity Fund. D.P.T. is an Alberta Heritage Foundation for Medical Research Scholar.

References and Notes

(1) Eldho, N. V.; Feller, S. E.; Tristram-Nagle, S.; Polozov, I. V.; Gawrisch, K. *J. Am. Chem. Soc.* **2003**, *125(21)*, 6409−6421.
(2) Feller, S. E.; Gawrisch, K.; MacKerell, A. D. *J. Am. Chem. Soc.* **2002**, *124(2)*, 318−326.
(3) Huber, T.; Rajamoorthi, K.; Kurze, V. F.; Beyer, K.; Brown, M. F. *J. Am. Chem. Soc.* **2002**, *124(2)*, 298−309.
(4) Forrest, L. R.; Sanson, M. S. P. *Curr. Opin. Struct. Biol.* **2000**, *10(2)*, 174−181.
(5) Nagle, J. F.; Tristram-Nagle, S. *Biochem. Biophys. Acta* **2000**, *1469 (3)*, 159−195.
(6) Drozdov, A. N.; Tucker, S. C. *J. Phys. Chem. B* **2002**, *106*, 515−516.
(7) Saiz, L.; Klein, L. *Biophys. J.* **2001**, *81*, 204−216.
(8) Stillwell, W.; Wassall, S. R. *Chem. Phys. Lipids* **2003**, *126*, 1−27.
(9) Hyvönen, M. T.; Rantala, T. T.; Ala-Korpela, M. *Biophys. J.* **1997**, *73*, 2907−2923.
(10) Hyvönen, M. T.; Ala-Korpela, M.; Rantala, T. T.; Jokisaari, J. *Chem. Phys. Lett.* **1997**, *268*, 55−60.
(11) Hyvönen, M. T.; Hiltunen, Y.; El-Deredy, W.; Ojala, T.; Vaara, J.; Kovanen, P. T.; Ala-Korpela, M. *J. Am. Chem. Soc.* **2001**, *123*, 810−816.
(12) Feller, S. E. *J. Phys. Chem. B* **2000**, *104*, 7510−7515.
(13) Scott, E. F.; Gawrisch, K.; MacKerell, A. D., Jr. *J. Am. Chem. Soc.* **2002**, *124*, 318−326.
(14) Tieleman, D. P.; Marrink, S. J.; Berendsen, H. J. C. *Biochim. Biophys Acta* **1997**, *1331*, 235−270.
(15) Chiu, S. W.; Jakobsson, E.; Mashl, R. J.; Scott, H. L. *Biophys. J.* **2002**, *83*, 1842−1853.
(16) Brodnitz, M. H. *J. Agric. Food Chem.* **1968**, *16*, 994−999.
(17) Tian, K.; Dasgupta, P. K. *Anal. Chem.* **1999**, *71*, 1692−1698.
(18) Vallve, J. C.; Uliaque, K.; Girona, J.; Cabre, A.; Ribalta, J.; Heras, M.; Masana, L. *Atherosclerosis* **2002**, *164(1)*, 45−56.
(19) Mattson, M. P.; Cheng, B.; Davis, D.; Bryant, K.; Lieberburg, I.; Rydel, R. E. J. *Neuroscience* **1992**, *12*, 376−389.
(20) Murphy, R. C. *Chem. Res. Toxicol.* **2001**, *14(5)*, 463−472.
(21) Burgisser, P.; Matthieu, J. M. *Neurochem. Res.* **1989**, *14(1)*, 91−96.
(22) Labuza, T. P. *Crit. Rev. Food Technol.* **1971,** *2*, 365−368.
(23) Nieuwenhuizen, W. F.; van Lenthe, J. H.; Blomsma, E. J.; Van der Kerk, V.; Hoof, A. C.; Veldink, G. A.; Vliegenthart, J. F. *Free Radical Biol. Med.* **1997**, *22(6)*, 1101−1108.
(24) Pratt, D. A.; Mills, J. H.; Porter, N. A. *J. Am. Chem. Soc.* **2003**, *123*, 5801−5810.
(25) Frisch, M. J.; Trucks, G. W.; Schlegel, H. B.; Scuseria, G. E.; Robb, M. A.; Cheeseman, J. R.; Zakrzewski, V. G.; Montgomery, J. A., Jr.;

Stratmann, R. E.; Burant, J. C.; Dapprich, S.; Millam, J. M.; Daniels, A. D.; Kudin, K. N.; Strain, M. C.; Farkas, O.; Tomasi, J.; Barone, V.; Cossi, M.; Cammi, R.; Mennucci, B.; Pomelli, C.; Adamo, C.; Clifford, S.; Ochterski, J.; Petersson, G. A.; Ayala, P. Y.; Cui, Q.; Morokuma, K.; Malick, D. K.; Rabuck, A. D.; Raghavachari, K.; Foresman, J. B.; Cioslowski, J.; Ortiz, J. V.; Stefanov, B. B.; Liu, G.; Liashenko, A.; Piskorz, P.; Komaromi, I.; Gomperts, R.; Martin, R. L.; Fox, D. J.; Keith, T.; Al-Laham, M. A.; Peng, C. Y.; Nanayakkara, A.; Gonzalez, C.; Challacombe, M.; Gill, P. M. W.; Johnson, B. G.; Chen, W.; Wong, M. W.; Andres, J. L.; Head-Gordon, M.; Replogle, E. S.; Pople, J. A. *Gaussian 98*, revision A.11; Gaussian, Inc.: Pittsburgh, PA, 1998.

(26) Becke, A. D. *J. Chem. Phys.* **1993**, *98*, 5648−5652.

(27) OriginPro 7 is a product of OriginLab Corporation: Northampton, MA; website: http://www.originlab.com/.

(28) Marquardt, D. W. *J. Soc. Ind. Appl. Math.* **1963**. *11*, 431−441, 1963.

(29) van der Spoel, D.; van Buuren, A. R.; Apol, E.; Meulenhoff, P. J.; Tieleman, D. P.; Sijbers, A. L. T. M.; Hess, B.; Feenstra, K. A.; Lindhal, E.; van Drunen, R.; Berensden, H. J. C. *Gromacs User Manual*, version 3.1.1; Nijenborgh 4, 9747 AG Groningen: The Netherlands, 2002; www.gromacs.org.

(30) Tieleman, D. P.; Sansom, M. S. P.; Berendsen, H. J. C. *Biophys. J.* **1999**, *76*, 40−49.

(31) Essmann, U.; Perera, L.; Berkowitz, M. L. *J. Chem. Phys.* **1995**, *103*, 8577−8593.

(32) Hess, B.; Bekker, H.; Berendsen, H. J. C.; Fraaije, J. G. E. M. *J. Comput. Chem.* **1997**, *18*, 1463−1472.

(33) Berendsen, H. J. C.; Postma, J. P. M.; van Gunsteren, W. F.; DiNola, A.; Haak, J. R. *J. Chem. Phys.* **1984**, *81*, 3684−3690.

(34) Berger, O.; Edholm, O.; Jahnig, F. *Biophys. J.* **1997**, *72*, 2002−2013.

(35) Marrink, S. J.; Berger, O.; Tieleman, D. P.; Jahnig, F. *Biophys. J.* **1998**, *74*, 931−943.

(36) Berendsen, H. J. C.; van der Spoel, D.; van Drunen, R. *Comput. Phys. Comm.* **1995**, *95*, 43−56.

(37) Tieleman, D. P.; Bentz, J. *Biophys. J.* **2002**, *83*, 1501−1510.

(38) Hermans, J.; Berendsen, H. J. C.; van Gunsteren, W. F.; Postma, J. P. M. *Biopolymers* **1984**, *23*, 1513−1518.

(39) Coordinate files and parameters are available from Biocomputing at the University of Calgary website, managed by D.P.T.: http:// moose .bio.ucalgary.ca.

(40) Cantor, R. S. *Biophys. J.* **1999**, *76(5)*, 2625−2639.

(41) Mashl, R. J.; Scott, H. L. *Biophys. J.* **2001,** *81*, 3005−3015.

(42) Binder, H.; Gutberlet, T.; Anikin, A.; Klose, G. *Biophys. J.* **1998**, *74*, 1908−192.

(43) Chiu, S. W.; Jakobsson, E.; Subramaniam, S.; Scott, H. L. *Biophys. J.* **1999**, *77*, 2462−2469.

(44) Murzyn, K.; Róg, T.; Jezierskin, G.; Takaoka, Y.; Pasenkiewicz-Gierula, M. *Biophys. J.* **2001**, *81*, 170−183.

(45) Nagle, J. F.; Tristram-Nagle, S. *Curr. Opin. Struct. Biol.* **2000**, *10*, 474−480.

(46) Dominguez, H.; Smondyrev, A. M.; Berkowitz, M. L. *J. Phys. Chem. B* **1999**, *103(44)*, 9582−9588.

(47) Seelig, J.; Waespe S. *Biochemistry* **1978**, *17*, 3310−3315.

(48) Holte, L. L.; Peter, S. A.; Sinnwell, T. M.; Gawrisch, K. *Biophys. J.* **2003**, *68*, 2396−2403.

(49) Feller, S. E.; Yin, D. X.; Pastor, R. W.; Mac-Kerell, A. D. *Biophys. J.* **1997**, *73*, 2269−2279.

(50) Rickard, G.; Brunelle, P.; Bachar, M.; Rauk, A. to be published.